Journal of Materials Chemistry A

Accepted Manuscript

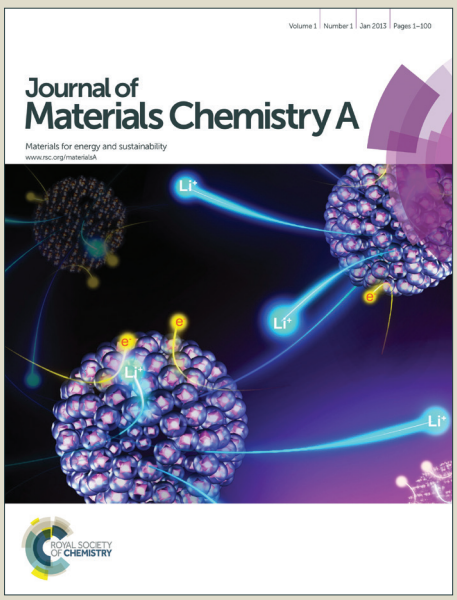

ROYAL SOCIETY OF CHEMISTRY

www.rsc.org/materialsA

Preparation of reduced graphene oxide-$Ni(OH)_2$ composites by electrophoretic deposition: Application for non-enzymatic glucose sensing

Palaniappan Subramanian,[1] Joanna Niedziolka-Jonsson,[1] Adam Lesniewski,[1] Qian Wang,[1,3] Musen Li,[3] Rabah Boukherroub[2] and Sabine Szunerits[2]*

[1] *Institut de Recherche Interdisciplinaire (IRI, USR-3078), Université Lille 1, Parc de la Haute Borne, 50 avenue de Halley, BP 70478, 59658 Villeneuve d'Ascq, France*

[2] *Institute of Physical Chemistry, Polish Academy of Sciences, Kasprzaka 44/52, 01-224 Warszawa, Poland*

[3] *Key Laboratory for Liquid-Solid Structural Evolution and Processing of Materials (Ministry of Education), Shandong University, Jinan 250061, China*

Abstract

A sensitive and stable non-enzymatic sensing platform for D-glucose based on a reduced graphene oxide (rGO) matrix modified with $Ni(OH)_2$ nanostructures was established. The sensing matrix was fabricated in one-step through an electrophoretic deposition approach. It is based on the mixing of negatively charged graphene oxide (GO) with nickel ions resulting in a positively charged composite making cathodic electrophoretic deposition possible. The thickness of the resulting rGO/$Ni(OH)_2$ matrix deposited on Au could be controlled by varying the time of electrophoretic deposition. The rGO/$Ni(OH)_2$ matrix was characterized by X-ray photoelectron spectroscopy, Raman spectroscopy and cyclic voltammetry. The rGO/$Ni(OH)_2$ electrodes exhibited excellent electrocatalytic behaviour towards oxidation of glucose in alkaline medium. The response current of the sensor is linear to glucose concentrations from 15 µM to 30 mM with a sensitivity to glucose of 11.4±0 mA cm^{-2} mM^{-1}. The interface was much more stable then drop casted films. These results pave the way for electrophoretic deposition as competitive alternative over drop casting for the fabrication of rGO modified interfaces.

Key words: reduced graphene oxide, nickel hydroxide, glucose, enzyme-free, amperometic sensor

1. Introduction

Diabetes is, next to cancer, cardiovascular and chronic respiratory diseases, one of the first four leading causes of death and disability.[1] A close monitoring of the blood glucose concentration can largely control and manage diabetes. Tremendous efforts have been put into the development of efficient and reliable methods for glucose sensing.[2-4] Glucose oxidase-based biosensors have been developed for this purpose and amperometic enzyme electrodes have played a leading role in the move to simple easy-to-use blood sugar testing.[1, 4] While these enzyme-based electrochemical sensors are dominating the market, they suffer from various drawbacks originating from the instability of the enzyme causing a significant problem to most sensor designs.[5, 6]An attractive alternative to overcome some of the limitations of enzymatic biosensors relies on the development of non-enzymatic glucose sensors.[7-13] Although, these sensors are somewhat nonselective towards other carbohydrates such as fructose and sucrose and need to be for the most part operated in an alkaline medium, they display a lot of advantages such as fast response time, higher sensitivity and better stability than glucose oxidase-based interfaces. Among the proposed nanomaterials, copper and nickel oxides have especially received much attention for nonenzymatic glucose sensing in alkaline media.[14-19] The electrochemical oxidation of glucose by the $Ni(OH)_2$/NiOOH redox couple formed on the electrode surface in alkaline medium makes nickel of particular interest.[8, 20, 21] The excellent electrocatalytic properties together with nickel being a relative low cost material makes it an adequate choice for the development of enzyme-free glucose sensors.

An emerging new type of supporting substrates for nanomaterials is graphene and its derivatives.[22] Loading metal nanoparticles on conductive graphene nanosheets gives rise to nanocomposites with larger active surface areas and improved electron transport, making the nanocomposites ideal materials for the fabrication of electrochemical sensors.[9, 23-25] Recent works have shown that graphene and its derivatives can be modified in different ways with $Ni(OH)_2$ nanostructures.[12, 26-33] The interest in such graphene decorated with $Ni(OH)_2$ nanostructures was mostly related to the development of energy devices as $Ni(OH)_2$ has been a primary electrode material in alkaline batteries and is an attractive candidate for supercapacitance applications. The preparation methods of the nanocomposites are mainly two-step procedures involving the chemical reduction and exfoliation of graphene oxide or the direct use of graphene and loading with the metal nanoparticles of interest.[34, 35] One-step approaches consisting of simultaneous

reduction of GO and particle deposition are straightforward green approaches towards the formation of such nanocomposites free of chemical reducing agents and organic linkers commonly used to attach metal nanoparticles.[25, 36]

Here we report on the fabrication and characterization of $Ni(OH)_2$ nanostructures modified rGO matrices using electrophoretic deposition (EPD) and their use for highly sensitive non-enzymatic glucose detection. EPD offers several advantages over other surface coating approaches, such as process simplicity, uniformity of the deposited films and good control of the deposited thickness. All these attributes can be exploited for the preparation of rGO films on interfaces.[37-41] Wu et al. pioneered the EPD process of graphene films showing that Mg^{2+} charged GO can be deposited on a cathode electrode under applied voltage at 100-160 V.[37] The group of Ruoff et al. demonstrated that uniform, thickness adjustable graphene films can be obtained by controlled EPD of hydrazine or KOH modified GO.[41] We have recently shown that nanometer thick rGO films can be formed on gold interfaces using EPD. Using an aqueous GO suspension of 0.5 mg/mL and a DC potential of 150 V for 20s allowed deposition of about 2 nm thick rGO films (corresponding to 5-6 graphene layers) on gold electrodes in a highly reproducible manner.[38] The access to a simple, reproducible and controllable technique to produce rGO coatings of thicknesses from the low nanometer to the millimeter range makes EPD a promising alternative to other coating strategies of electrodes, in particular drop-casting, most widely used for electrochemical applications. The electrochemical behavior of electrodes modified by drop-casting is representative of the electrochemical behavior from numerous graphene fragments with ill-defined coverage, layer numbers and orientation, with possible interference from exposed areas of the underlying electrode. Such interfaces are often graphite-like as the number of graphene sheets exceeds large 100 sheets. A method like EPD reducing the thickness of rGO coatings in a controlled manner could be highly beneficial for the construction of electrochemical sensors.

2. Experimental Section

2.1. Materials

Graphite powder (< 20 micron), potassium permanganate ($KMnO_4$), sulphuric acid (H_2SO_4), hydrogen peroxide (H_2O_2), nickel chloride hexahydrate ($NiCl_2.6H_20$), sodium hydroxide (NaOH), sodium borohydride ($NaBH_4$), dimethylformamide (DMF), glucose, uric acid (UA),

ascorbic acid (AA), dopamine hydrochloride (DA) and ethanol were purchased from Sigma-Aldrich Corporation. All chemicals were reagent grade or higher and were used as received unless otherwise specified. The aqueous solutions used in the experiments were prepared using Milli-Q water.

2.2. Preparation of graphene oxide (GO)

Graphene oxide (GO) was synthesized from graphite powder by a modified Hummers method.[42] 5 mg of the synthesized GO was dispersed in 1 mL of water and exfoliated through ultrasonication for 3 h. This aqueous suspension of GO was used as a stock suspension in subsequent experiments.

2.3. Preparation of reduced graphene oxide (rGO)

In a typical procedure, hydrazine hydrate (0.50 mL, 32.1 mM) was added to 5 mL of the yellow-brown GO aqueous suspension (0.5 mg/mL) in a round bottom flask and heated in an oil bath at 100°C for 24 h over which the reduced GO gradually precipitated out the solution. The product was isolated by filtration over a PVDF membrane with a 0.45 μm pore size, washed copiously with water (5×20 mL) and methanol (5×20 mL), and dried.[43].

2.4. Preparation of rGO modified gold interfaces by drop-casting

rGO modified gold electrodes were prepared by casting five times 10 μL of a DMF solution of rGO (0.5 mg/mL) onto gold followed by subsequent drying at 70°C in an oven for 24 h.

2.5. Preparation of rGO modified gold interfaces by electrophoretic deposition

The electrophoretic deposition was carried out using a two-electrode cell containing the GO aqueous dispersion (0.5 mg/mL) by applying DC voltage (150 V) for 20 s. Platinum (Pt) foil (1 × 2 cm^2) acts as the cathode and the gold as the anode. The two electrodes are separated by 1 cm and are placed parallel to each other in the GO dispersion. After deposition, the interface was washed with deionized water (three times) followed by blow drying with nitrogen.

2.6. One-step electrophoretic deposition of $Ni(OH)_2$ and rGO/$Ni(OH)_2$

Electrophoretic deposition was performed on gold coated glass substrates prepared by thermal evaporation of 5 nm of titanium and 50 nm of gold onto cleaned glass slides (76×26×1mm^3, CML France). The electrophoretic deposition is carried out in a two-electrode cell, where the two electrodes are placed parallel to each other and are separated by a distance of 1cm. A platinum foil (1x2 cm^2) acts as the cathode and the gold substrate as the anode. GO and GO/$NiCl_2$ suspensions were ultrasonicated for 30 min before use. The electrophoretic cell was then filled with a solution of GO (0.6 mg/mL) or GO (0.6 mg/mL)/ $NiCl_2.6H_2O$ (0.6 mg/mL) in a 1:1 mixture of both in ethanol and a DC voltage of 50 V was applied for 20 s. After deposition, the interfaces were rinsed with deionized water (three times) followed by blow drying with nitrogen. Enrichment of the $Ni(OH)_2$ layer in the composite film was accomplished by cycling the film 300 times in 0.1 M NaOH between 0 and +0.8 V.

2.7. Characterization

X-ray photoelectron spectroscopy (XPS)

X-ray photoelectron spectroscopy (XPS) experiments were performed in a PHl 5000 VersaProbe - Scanning ESCA Microprobe (ULVAC-PHI, Japan/USA) instrument at a base pressure below 5×10^{-9} mbar. Monochromatic AlK_α radiation was used and the X-ray beam, focused to a diameter of 100 μm, was scanned on a 250×250 μm surface, at an operating power of 25 W (15 kV). Photoelectron survey spectra were acquired using a hemispherical analyzer at pass energy of 117.4 eV with a 0.4 eV energy step. Core-level spectra were acquired at pass energy of 23.5 eV with a 0.1 eV energy step. All spectra were acquired with 90° between X-ray source and analyzer and with the use of low energy electrons and low energy argon ions for charge neutralization. After subtraction of the Shirley-type background, the core-level spectra were decomposed into their components with mixed Gaussian-Lorentzian (30:70) shape lines using the CasaXPS software. Quantification calculations were conducted with using sensitivity factors supplied by PHI.

Scanning electron microscopic (SEM) and energy dispersed X-ray (EDX)

Scanning electron microscopic images and energy dispersive X-ray spectroscopy (EDX) spectra of the films were obtained using FEI Nova NanoSEM 450 scanning electron microscope with

FEG (field emission gun, Schottky type) systems equipped with an energy dispersive X-ray analyzer at an accelerating voltage of 20 kV.

Electrochemical measurements

Electrochemical experiments were performed using an Autolab potentiostat 20 (Eco Chemie, Utrecht, The Netherlands). Ag/AgCl (Bioanalytical Systems, Inc.) electrode was used as reference electrode, and platinum wire as counter electrode. Cyclic voltammetry (CV) measurements were performed in aqueous solutions of 0.1 M NaOH in the absence and presence of glucose on differently formed glass/Ti/Au/GO-$Ni(OH)_2$ films.

Chronoamperometric detection of glucose on glass/Ti/Au/GO-$Ni(OH)_2$ electrode was performed under N_2-saturated steady-state condition in stirring alkaline solution (0.1 M NaOH) by applying a constant potential of +0.6 V to the working electrode. When the background current became stable (after 100 s), a subsequent addition of glucose was realized and the current was measured.

3. Results and Discussion

We have recently shown that nanometer thick rGO films can be formed on gold interfaces using electrophoretic deposition (EPD) and can be used for plasmonic sensing.[38] As the zeta-potential of GO is -35 mV, anodic deposition of rGO rather than GO took place as previously shown by An et al.[44]. The formation of these rGO nanocomposite interfaces is highly reproducible and can be a competitive alternative to other rGO depositon methods, notably drop-casting. The electrochemical properties of gold electodes modified with chemically formed rGO and of gold electrodes mofidied with electrophoretically formed rGO using an aqueous GO suspension of 0.5 mg/mL and a DC potential of 150 V for 40 s were determined by cyclic voltammetry using $[Fe(CN)_6]^{3-/4-}$ as redox mediators (**Figure 1A**). Enhancement in the anodic and cathode peak currents are observed in both cases, suggesting that the gold/rGO interface exhibits better electrochemical activity than unmodified gold.[47] The ΔE_P is however larger for the gold/rGO interfaces formed through electrophoretic depositon. This might be due to the presence of more remaining oxygen functions on the rGO repelling the negatively charged $[Fe(CN)_6]^{3-/4-}$.

The stability of the rGO modified interfaces was investigated by cycling the electrode between -0.5V and 1.3 V in 0.1 M KCl, followed by recording CV in $[Fe(CN)_6]^{3-/4-}$. In the case of electrophoretically deposited rGO films, no change in the peak current height was observed after 100 cycles, while in the case of drop-casted rGO film, a 20 % current decrease was observed after 20 cycles. Electrophoretic deposition of rGO results in highly robust interfaces with long term stability and are thus well adapted for the construction of sensors. In the following such interfaces will be used for the construction of non-enzymatic glucose sensors.

3.1. Electrophoretic deposition of rGO/Ni(OH)$_2$ films onto gold electrodes

Several studies have demonstrated that direct non-enzymatic electrooxidation of glucose varied considerably with the electrode material used.[8-10, 13] Nickel nanostructures have shown to be particular suited for the fabriciton of non-enzyamtic glucose sensors[8, 11, 12, 32, 48-50] and will be used in this work to integrate into rGO matrixes formed by electrophoretic means. In the case of EPD deposition of rGO/Ni(OH)$_2$ films, charging GO with Ni^{2+} ions resulted in a nanocomposite with an overall positive zeta-potential (ζ=+14 mV) making cathodic rather than anodic EPD feasible (**Figure 2A)**. An ethanolic dispersed GO/Ni^{2+} was used as precursor for the formation of rGO/Ni(OH)$_2$ films on gold interfaces. The obtained suspension was stable enough for EPD due to the presence of residual polar oxygen-containing groups on the GO sheets. Application of a DC potential of +50 V for 10-60s resulted in the formation of porous rGO/Ni(OH)$_2$ films (**Figure 2B**) of increasing thickness (**Figure 1C**). Low-magntification SEM images of EPD films formed at different time scales indicate that rGO coated with nickel nanostructures are deposited during the process where the porosity changes as a function of deposition time (**Figure 2B)**. Longer deposition times gave layered structures with agglomerated rGO sheets on the top of the rGO/Ni(OH)$_2$ nanostructures. The film thickness varied between 500±150 nm (10 s deposition) to 3.1±0.3 μm (60 s) (**Figure 2C**).

The chemical composition of the rGO/Ni(OH)$_2$ composite (deposited for 60 s) was further examined by XPS and EDX, as shown in **Figure 3**. The Ni 2p XPS spectrum shows two major peaks centered at 856.1 and 873.6 eV with a spin-energy separation of 17.5 eV, corresponding to Ni $2p_{3/2}$ and Ni $2p_{1/2}$ respectively (**Figure 3A**). These bands are characteristic of Ni(OH)$_2$ phase,

in agreement with other literature reports.[29, 51] The two extra peaks centered at 861.1 and 879.5 correspond to Ni $2p_{3/2}$ and Ni $2p_{1/2}$ satellite peaks. The atomic percentage of nickel is 15.9 at. %. This is in accordance with EDX analysis where an atomic percentage of nickel of 16.15 at% was determined (**Figure 3B**). The C1s XPS spectrum of the rGO/$Ni(OH)_2$ film can be deconvoluted into four bands: the non-oxygenated sp^2 C-C (283.9 eV), sp^3 C-C and C-H (284.6 eV), C-O (286.1 eV) and C=O (288.2 eV) (**Figure 3C**). For comparison, the XPS spectrum of the initial GO nanosheets was included. The XPS spectrum of GO clearly shows a significant degree of oxidation with four components that correspond to carbon atoms of the different functional groups; sp^2 C-C (283.3 eV), sp^3 C-C and C-H (284.6 eV), C-O (286.5 eV) and C=O (287.9 eV). The increase of the C/O ratio in rGO/$Ni(OH)_2$ from 2.0 (GO) to 4.1 (except from oxygen atoms of $Ni(OH)_2$) is further evidence for the partial reduction of GO to rGO. EPD of rGO/$Ni(OH)_2$ films at 40 and 10 s respectively showed similar XPS results with nickel present is 12.9 at.% (10 s) and 15.5 at.% (40 s). Raman spectroscopy was in addition used to analyze the rGO/$Ni(OH)_2$ films. As shown in **Figure 3D**, the Raman spectrum of the rGO/$Ni(OH)_2$ films deposited by EPD at 50 V for 60 s displays a D-band at around 1350 cm^{-1}, a G-band a~1582 cm^{-2} and a broad 2D-band ~2700 cm^{-1}. In comparison to GO, the D- and G-bands are shifted to lower wavenumbers presumably resulting from the reduction of the GO platelets comprising the rGO/$Ni(OH)_2$ films.[44] EPD of rGO/$Ni(OH)_2$ films for 10 s and 40 s and showed comparable Raman characteristics (data not shown).

Before investigation of the electrocatalytic properties of the rGO/$Ni(OH)_2$ matrix, cyclic voltammograms of the novel hybrid were recorded from -0.2 V to +1V at various scan rates in alkaline solution (**Figure 4A**). The broad redox current peaks observed correspond to the $Ni(OH)_2$/NiOOH redox couple according to equation 1.

$$Ni(OH)_2 + OH^- \rightarrow NiOOH + H_2O + e^- \qquad (1)$$

The presence of $Ni(OH)_2$ and not exclusively nickel metal is well established in the literature as nickel forms spontaneously $Ni(OH)_2$ in aerated and alkaline solutions.[28, 30, 52] Electrodeposition of $Ni(OH)_2$ leads normally to the formation of two crystallographic phases, the hydrated α- $Ni(OH)_2$ and anhydrous β-$Ni(OH)_2$ form.[12 53] The anhydrous β-$Ni(OH)_2$ is the more stable of the two with a structure of nickel with octahedral coordination to eight oxygen atoms. After 300 cycles of the rGO/$Ni(OH)_2$ matrix in high NaOH concentration, only one oxidative peak is clearly present,

indicating the domination of β-$Ni(OH)_2$ films. The redox current observed on the rGO/$Ni(OH)_2$ matrix scales linearly with the square route of scan rate (**Figure 4B**), something already observed by Mu et al.[8] This linearity might indicate a diffusion controlled process involving OH^- diffusion from the supporting electrolyte to the electrode surface during the reduction step and from the electrode to the solution during the oxidation step.

3.3. Enzyme-less glucose sensor

The electrocatalytic performance of the rGO/$Ni(OH)_2$ matrix deposited at +50 V for 60 s towards glucose oxidation in alkaline medium is exhibited in **Figure 5A**. Addition of glucose (1 mM) results in a significant increase of the oxidation current of $Ni(OH)_2$/NiOOH redox couple. This is due to the change in the $Ni^{2+/}Ni^{3+}$ concentration ratio as a result of the rapid electrocatalytic oxidation of glucose following equation 2. After electrooxidation of $Ni(OH)_2$ to NiOOH in alkaline solution (equation 1), glucose can be oxidized to gluconic acid by NiOOH, which is reduced back to $Ni(OH)_2$ at the same time. The recycling results in the increase of the oxidation current. Indeed, in a control experiment using electrophoretically deposited rGO without the presence of Ni^{2+} salt no electrocatalytic current for glucose oxidation was observed underlining the importance of $Ni(OH)_2$.

$$NiOOH + glucose \rightarrow Ni(OH)_2 + \ gluconic\ acid \qquad (2)$$

The effect of rGO on $Ni(OH)_2$ and the importane of the presence of rGO was in addition demonstrated by investigating the electrocatalytic behavior of an electrophoretically deposited $Ni(OH)_2$ film. In the case of EPD of $Ni(OH)_2$ from $NiCl_2$, the deposition occured on the cathode due to the positive zeta potential of $NiCl_2$ solution. The morphology of the film is depicted in the inset of **Figure 5B**. Wire-like structures composed of interconnected flower like nanoparticles are seen in the case of $Ni(OH)_2$ composites. Comparision of the electrocatalytic behavior of glucose (1 mM) on $Ni(OH)_2$ film and rGO/ $Ni(OH)_2$ composite electrodes evidences that the electrocatalytic reaction is less marked on $Ni(OH)_2$ films, indicating the importance of the rGO matrix.

To confirm the use of this porous interface for amperometric glucose sensing in alkaline medium, the dynamic steady-state current response of the interface to successive additions of glucose was monitored. **Figure 5A** shows a typical current-time plot of the rGO/$Ni(OH)_2$ interface upon successive additions of 100 μM glucose when the interface was biased at +0.6 V. The amperometric response shows a staircase-like increase upon addition of glucose with a very fast response time towards the oxidation of glucose. The electrode responses immediately upon glucose addition and reaches its steady-state level within ≈7 s; this is ascribed to the good electrocatalytic properties of rGO/$Ni(OH)_2$. From the calibration curve (**Figure 5B**), an excellent linearity (R^2=0.999) over a wide concentration range of 0.02-30 mM with a slope of 10.0±0.5 mA cm^{-2} mM^{-1} was obtained. The detection limit of the electrode was found to be 20 μM at a S/N=3. **Table 1** summarizes the analytical parameters for gold electrodes modified with rGO/$Ni(OH)_2$ films for shorter EPD times. A somewhat better detection limit of 15 μM was recorded on the thinner films, with a slightly better sensitivity of 11.4±0 mA cm^{-2} mM^{-1}. The influence of the film thickness on the overall performance of the non-enzymatic sensor is low. The performance was compared to other non-enzymatic and enzymatic methods for glucose determination reported previously (**Table 2**). The detection limit is higher when compared to free-standing nickel oxide nanoflake arrays (LOD= 1.2 μM) with however a comparable glucose sensitivity (8.5 mA cm^{-2} mM^{-1}).[50] In comparison to an assembly of $Ni(OH)_2$ nanoplates on rGO formed by drop-casting of a chemically formed rGO/$Ni(OH)_2$ nanocomposite a better sensitivity was observed with a linear range shifted to higher glucose concentrations (**Table 2**).[32] One of the main advantages of the rGO/$Ni(OH)_2$ interface on gold is its long term stability. Loss of electro-catalytic activity toward addition of 1 mM glucose was about 7 % after 100 repetitive experiments, pointing towards a high stability of the interface over time.

One challenge in non-enzymatic glucose detection is specificity as other organic substances could simultaneous oxidize at the applied potential of +0.6 V. The effects of common interfering species including ascorbic acid, uric acid and dopamine were investigated in detail (**Figure 6**). While coexisting together with glucose in real samples, the concentrations of these species are much lower than glucose. As shown in **Figure 6,** no obvious current response was observed upon addition of the interfering species allowing thus an accurate and selective nonenzymatic detection of glucose.

The reproducibility and repeatability of the sensor was investigated by testing the amperometric current response of four fabricated rGO/$Ni(OH)_2$ interfaces to 1 mM glucose addition. A relative standard deviation of 6.2 % of the amperometric response was observed. Long-term stability of the sensor to glucose was in addition evaluated and the amperometric current shows a loss of 2% when testing a 1 mM glucose solution after the electrode had been stored at ambient temperature for a month.

4. Conclusion

In summary, $Ni(OH)_2$-reduced graphene oxide composites were developed through a facile and green one-step electrophoretic deposition approach. Application of a DC potential of +50 V on gold electrodes resulted in the formation of porous rGO/$Ni(OH)_2$ films with thicknesses varying from 500 nm to 3.1 µm. The rGO/$Ni(OH)_2$ electrodes exhibited excellent electrocatalytic behaviour towards oxidation of glucose in alkaline medium. Upon glucose addition steady-state levels were reached within ≈7 s. The interface showed a linear behavior over a wide concentration range with a sensitivity towards glucose of 11.4±0 mA cm^{-2} mM^{-1} and limit of detection of 15 µM. The sensor performance was not drastically influence by the films thickness, which thinner films showing a somewhat better detection limit. The advantages of electrophoretically deposited rGO nanocomposites are linked to the formation of highly reproducible electrode matrixes, to the good mechanical adherence of the matrix and the resulting long time stability of the sensing layer. Electrophoretic deposition is thus a viable alternative over drop casting for the fabrication of rGO modified interfaces.

Acknowledgment

PS acknowledges the financial support by the European Commission in RTN-project MATCON (contract no. 238201)R.B. and S.S. gratefully acknowledge financial support from the Centre National de Recherche Scientifique (CNRS), the University Lille 1 and the Nord Pas de Calais region. S.S thanks the Institut Universitaire de France (IUF) for financial support. JNJ and AL thank the European Union FP7, under the grant REGPOT-CT-2011-285949-NOBLESSE for financial support.

References

1 Z. Zhu, L. Garcia-Gancedo, A. J. Flewitt, H. Xie, F. Moussy and W. I. Milne, *Sensors* 2012, 12, 5996.
2 Y. Liu, V. Javvaji, S. R. Raghavan, W. E. Bentley and G. F. Payne, *J Agric Food Chem.*, 2012, 12, 8963.
3 J. Wang, D. F. Thomas and A. Chen, *Anal. Chem.*, 2008, 80, 997.
4 J. Wang, *Chem. Rev.*, 2008, 108, 814.
5 M. Lopez, S.-P. Mecerreyes, D. Lopez-Cabarcos and E. B. Lopez-Ruiz, *Biosens. Bioelectron.*, 2006, 21, 2320.
6 H. Muguruma and Y. Kase, *Biosens. Bioelectron.*, 2006, 22, 737.
7 Y. Bai, Y. Sun and C. Sun, *Biosens. Bioelectron.*, 2008, 24, 579.
8 Y. Mu, D. Jia, Y. He, Y. Mia and H.-L. Wu, *Biosens. Bioelectron.*, 2011, 26, 2948.
9 Q. Wang, I. Kaminska, J. Niedziolka-Jonsson, M. Opallo, L. Musen, R. Boukherroub and S. Szunerits, *Biosens. Bioelectron.*, 2013, 50, 331-337.
10 Q. Wang, P. Subramanian, M. Li, W. S. Yeap, K. Haenen, Y. Coffinier, R. Boukherroub and S. Szunerits, *Electrochem. Commun.*, 2013, 34, 286.
11 N. Yang, W. Smirnov and C. E. Nebel, *Electrochem. Commun.*, 2013, 27, 89.
12 B. Yuan, C. Xu, D. Deng, Y. Xing, L. Liu, H. Pang and D. Zhang, *Electrochim. Acta*, 2013, 88, 708.
13 S. Park, H. Boo and T. D. Chung, *Anal. Chim. Acta*, 2006, 556, 46.
14 A. R. M. Hameed, *Biosens. Bioelectron.*, 2013, 47, 248.
15 X. Kong, J. Zhao, W. Shi and M. Wei, *Electroanalysis*, 2013, 25, 1594.
16 W. Lu, X. Qin, A. M. Asiri, A. O. Al-Youbi and X. Sun, *Analyst*, 2013, 138, 429.
17 D. C. Marcano, D. V. Kosynkin, J. M. Berlin, S. Sinitskii, Z. Sun, A. Slesarev, L. B. Alemay, W. Lu and J. M. Tour, *ACS Nano*, 2010, 4, 4806.
18 V. Scognamiglio, *Biosens. Bioelectron.*, 2013, 47, 12.
19 X. Wang, X. Dong, Y. Wen, C. Li, Q. Xiong and P. Chen, *Chem. Commun.*, 2012, 48, 6490.
20 A. Safavi, N. Maleki and E. Farjami, *Biosens. Bioelectron.*, 2009, 24, 1655.
21 K. E. Toghill, L. Xiao, M. A. Phillips and R. G. Compton, *Sens. Actuators B*, 2010, 147, 642.
22 H. Park and R. S. Ruoff, *Nature Nanotechnol.*, 2009, 4, 217.
23 C. S. Shan, H. F. Yang, D. X. Han, Q. Zhang, A. Ivaska and L. Niu, *Biosens. Bioelectron.*, 2010, 25, 1070.
24 Q. Wang, M. R. Das, M. Li, R. Boukherroub and S. Szunerits, *Bioelectrochemistry*, 2013, 93, 15-22.
25 H. Gao, F. Xia, C. B. ching and H. Duan, *ACS Appl. Mater. Interfaces*, 2011, 3, 3049.
26 H. L. Wang, H. S. Casalongue, Y. Liang and H. Dai, *J. Am. Chem. Soc*, 2009, 132, 7472.
27 H. L. Wang, J. T. Robinson, G. Diankov and H. Dai, *J. Am. Chem. Soc*, 2010, 132, 3270.
28 Xu, X. Huang, Z. Lin, X. Zhong, Y. Huang and X. Duan, *Nano Res.*, 2013, 6, 65.
29 H. Yan, J. Bai, X. Zhang, B. Wang, Q. Liu and L. Liu, *Cryst. Eng. Comm.*, 2013, DOI: 10.1039/C3CE41361F.
30 J. Q. Xie, X. Sun, N. Zhang, K. Xu, M. Zhaou and Y. Xie, *Nano Energy*, 2013, 2, 65.
31 Y. Q. Zhang, Y. Z. Wang, J. B. Jia and J. G. Wang, *Sens. Actuators B*, 2012, 171-172, 580.

32 Y. Zhang, F. G. Xu, Y. J. Sun, Y. Shi, Z. W. Wen and Z. Li, *J. Mater. Chem.*, 2011, 21, 16949.

33 X. C. Dong, H. WXu, X. W. Wang, X. Y. Huang, M. B. Chan-Park, H. Zhang, L. H. Wang, W. Huang and P. Chen, *ACS Nano*, 2012, 6, 3206.

34 G. Goncalves, P. Marques, C. M. Grandadeiro, H. I. S. Nogueira, M. K. Singh and J. Gracio, *Chem. Mater.*, 2009, 21, 4796.

35 s. Zhang, Y. Y. Shao, H. G. Liao, J. Liu, I. A. Aksay, G. P. Yin and Y. H. Lin, *Chem. Mater.*, 2011, 23, 1079.

36 Q. Wang, N. Plylahan, M. V. Shelke, R. Devarapalli, L. Musen, P. Subramanian, D. T., R. Boukherroub and S. Szunerits, *Carbon*, 2013, DOI:10.1016/j.carbon.2013.10.077.

37 Z.-S. Wu, S. Pei, W. Ren, D. Tang, L. Gao, B. Liu, F. Li, C. Liu and H.-M. Cheng, *Adv. Mater.*, 2009, 21, 1756.

38 P. Subramanian, A. Lesniewski, I. Kaminska, A. Vlandas, A. Vasilescu, J. Niedziolka-Jonsson, E. Pichonat, H. Happy, R. Boukherroub and S. Szunerits, *Biosens. and Bioelect.*, 2013, 50, 239.

39 H. Zhang, X. Zhang, D. Zhang, X. Sun, H. Lin, C. Wang and Y. Ma, *J. Phys. Chem. B*, 2013, 117, 1616.

40 Y. Chen, X. Zhang, P. Yu and Y. Ma, *Chem. Commun.*, 2009, 4527.

41 S. J. An, Y. Zhu, S. H. Lee, M. D. Stoller, T. Emilsson, S. Park, A. Velamakanni, J. An and R. S. Ruoff, *J. Phys. Chem. Lett.*, 2010, 1, 1259.

42 M. R. Das, R. K. Sarma, R. Saikia, V. S. Kale, M. V. Shelke and P. Sengupta, *Colloid Surf. B: Biointerfaces*, 2011, 83, 16.

43 S. Stankovich, D. A. Dikin, R. D. Piner, K. A. Kohlhaas, A. Kleinhammes, Y. Jia, Y. Wu, S. T. Nguyen and R. S. Ruoff, *Carbon*, 2007, 45, 1558.

44 S. J. An, Y. W. Zhu, S. H. Lee, M. D. Stoller, T. Emilsson, S. Park, A. Velamakanni, J. H. An and R. S. Ruoff, *J. Phys. Chem. Lett.*, 2012, 1, 1259.

45 P. Chen and R. L. McCreery, *Anal. Chem.*, 1996, 68, 3958.

46 Y. Shao, J. Wang, H. Wu, J. Liu, I. A. Aksay and Y. Lin, *Electroanalysis*, 2010, 22, 1027.

47 C. Zhu, S. W. Guo, Y. Fang and S. Dong, *ACS Nano*, 2010, 4, 2429.

48 V. A. Kumary, T. E. M. Nancy and K. Sreevalsan, *Int. J. Electrochem. Sci.*, 2013, 8, 2220.

49 N. Qiao and J. Zheng, *Microchim. Acta*, 2012, 177, 103.

50 G. Wang, X. Lu, T. Zhai, Y. Ling, H. L. Wang, Y. Tong and Y. Li, *Nanoscale*, 2012, 4, 3123.

51 J. W. Lee, T. Ahn, D. Soundararajan, J. M. Ko and J. D. Kim, *Chem. Commun.*, 2011, 47, 6305.

52 H. L. Wang, H. S. Casalongue, Y. Liang and H. Dai, *J. Am. Chem. Soc.*, 2010, 132, 7472.

53 K. E. Toghill, L. Xiao, N. R. Stradiotto and R. G. Compton, *Electroanalysis*, 2010, 22, 491.

54 M. Shamsipur, M. Naja and M. R. M. Hosseini, *Bioelectrochemistry*, 2010, 77, 120.

55 S. Alwarappan, C. Liu, A. Kumar and C. Li, *J. Phys. Chem. C*, 2010, 114, 12920.

Table 1: Comparison of analytical performance of the rGO/$Ni(OH)_2$ interfaces depending on deposition time.

Time (s)	Thickness (nM)	Linear range (mM)	Sensitivity (mA cm^{-2} mM^{-1})	LOD (µM)
10	520±150	0.01-30	11.4±0.3	15±3
40	2000±350	0.05-30	10.5±0.5	20±2
60	3150±300	0.02-30	10.0±0.8	20±3

Table 2: Comparison of analytical performance of other non-enzymatic and enzymatic glucose sensors.

material	Linear range (mM)	Sensitivity (mA cm^{-2} mM^{-1})	LOD (µM)	Ref.
NiO/MWCNT	0.001-5	0.43	160	[54]
rGO/PtNi	0.003-3	1.08	1	[12]
Graphene/GOD	-	-	3	[55]
Free standing NiO nanoflakes	0.01-0.8	8.5	1.2	[50]
rGO/$(NiOH)_2$ (drop casting)	0.002-3.1	0.01	0.6	[32]
Nano NiO	0.001-0.1	5.59	0.16	[8]
rGO/$(Ni\text{-}OH)_2$ (electrophoretic)	**0.02-30**	**11.4±0.3**	**15**	**this work**

GOD=glucose oxidase

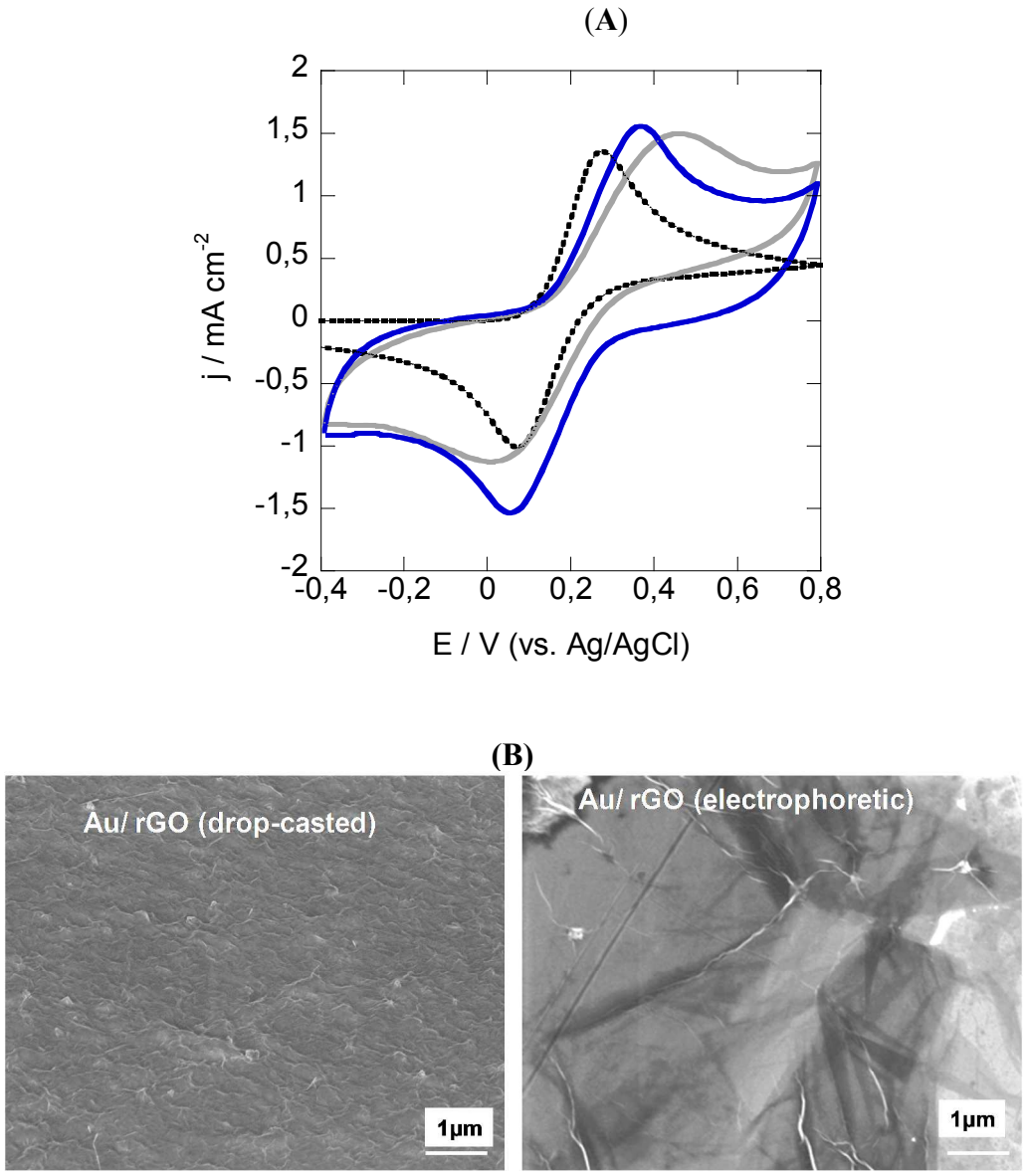

Figure 1: (A)Cyclic voltammograms obtained on gold (dotted black), gold/rGO formed by drop-casting (blue) and gold/rGO formed electrophoretically from a solution of 0.5 M GO (t=40 s, E=150 V) (grey) electrodes in 10 mM $[Fe(CN)_6]^{4-}$/ KCl (0.1 M), scan rate=50 mV s^{-1}, (C) SEM image of gold/rGO electrodes

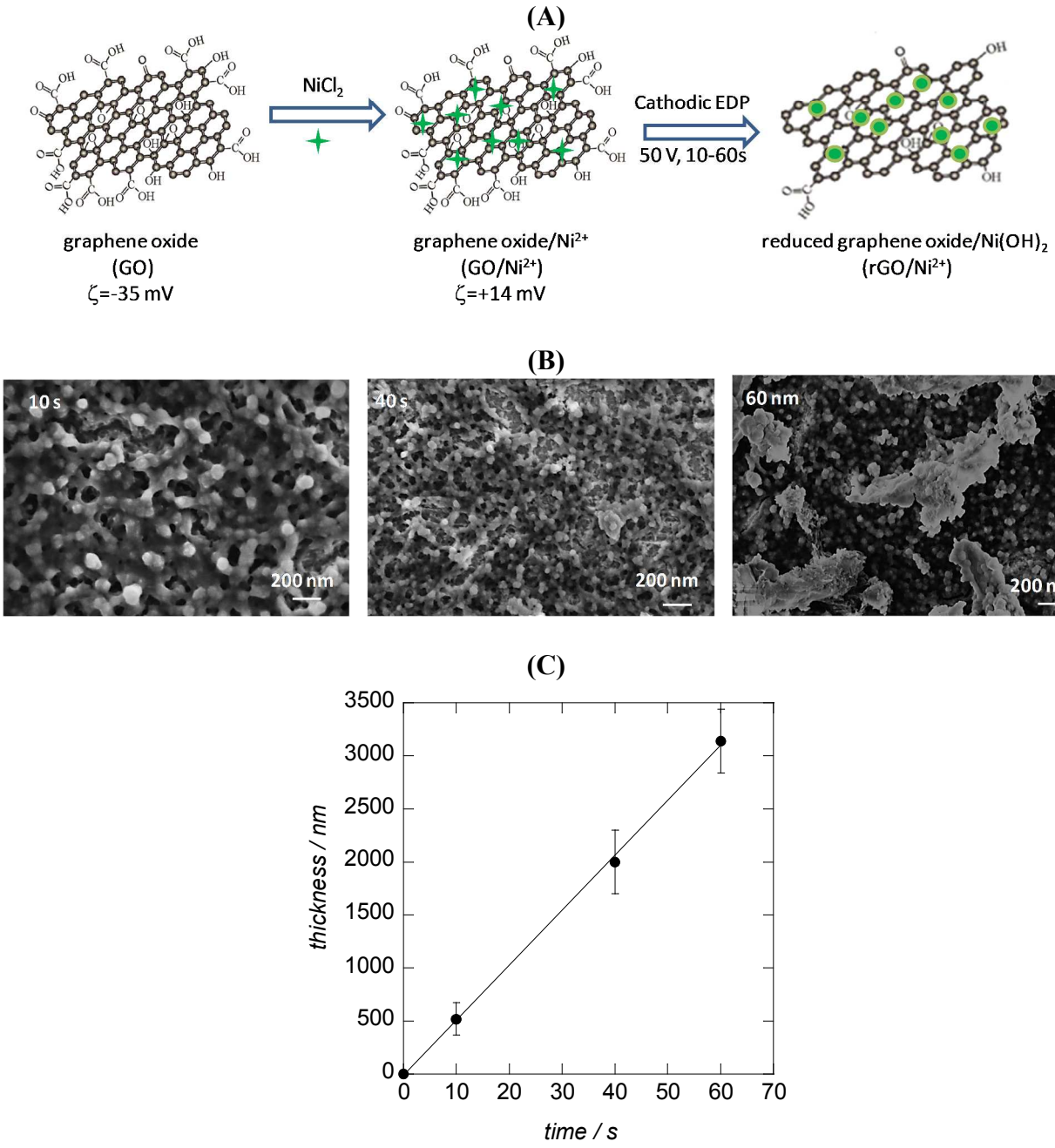

Figure 2: (A) Schematic diagram of EPD of rGO/$Ni(OH)_2$; (B) SEM images of the formed rGO/$Ni(OH)_2$ nanocomposite; (C) Influence of the deposition time on the thickness of the rGO/$Ni(OH)_2$ nanocomposite under a DC voltage of 50 V in ethanolic solution.

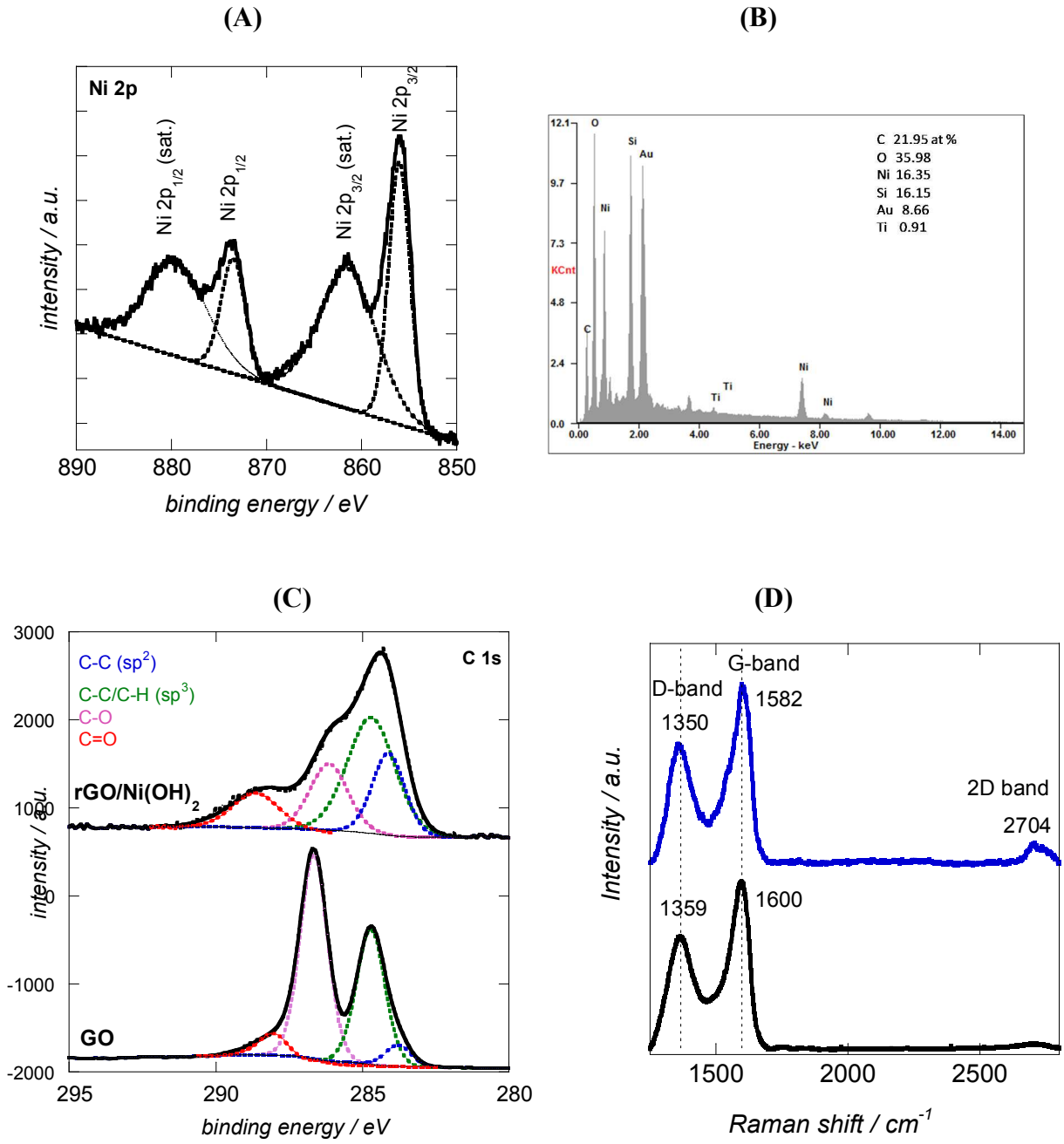

Figure 3: Characterisation of **r**GO/Ni(OH)$_2$ films deposited by EPD at 50 V for 60 s onto glass/Ti/Au interfaces: (A) Ni_{2p} high resolution XPS spectrum; (B) EDX spectrum; (C) C1s high resolution XPS spectrum of GO and GO/Ni(OH)$_2$; (D) Raman spectra of GO (black) and rGO/Ni(OH)$_2$ (blue).

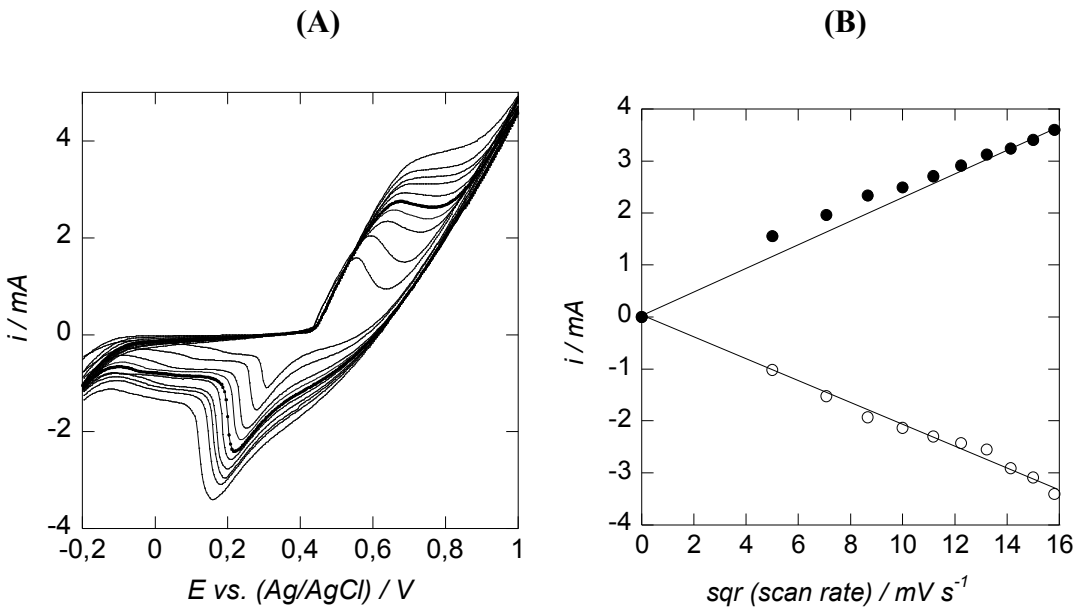

Figure 4: (A) Cyclic voltammograms of rGO/$Ni(OH)_2$ film on gold electrode at different scan rates in 0.1 M NaOH; (B) Change of peak current with square root of scan rate for anodic (●) and cathodic (o) currents.

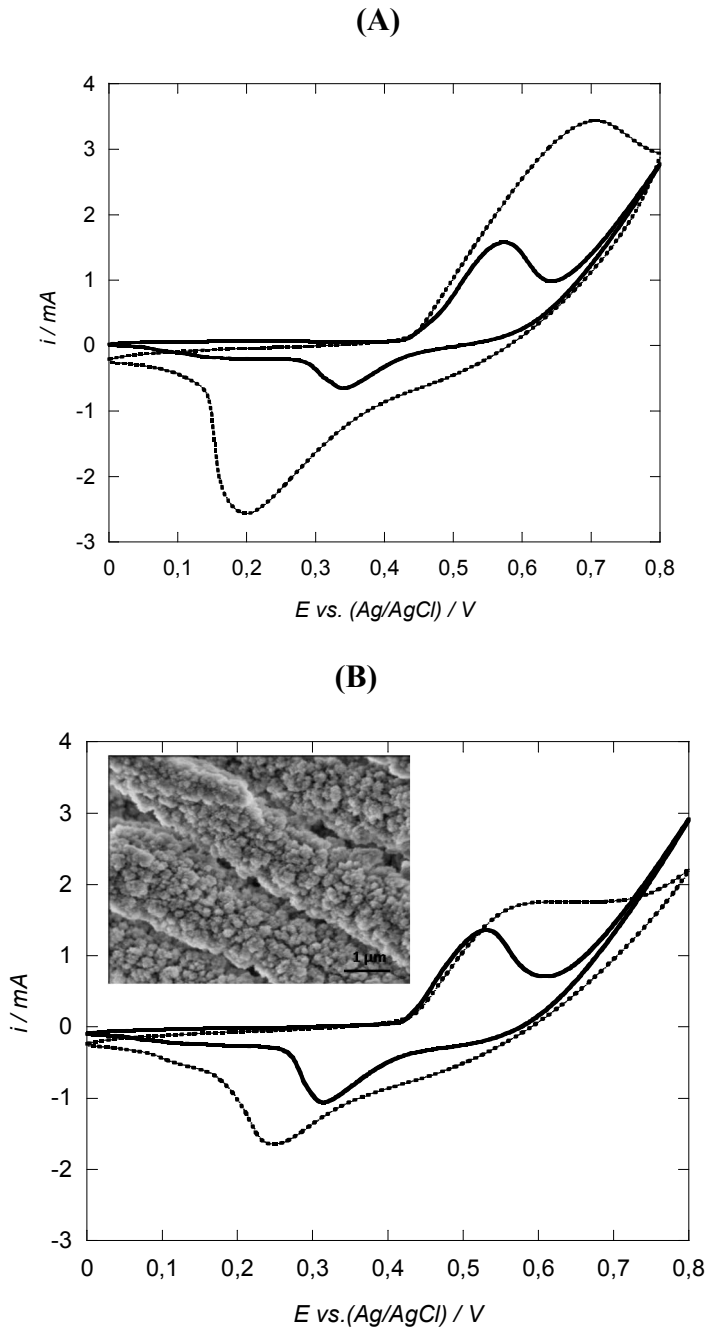

Figure 5: Cyclic voltammograms of (A) rGO/$Ni(OH)_2$ modified gold electrode and (B) $Ni(OH)_2$ modified electrodes (inset: SEM image) in 0.1 M NaOH before (full line) and after addition of 1 mM glucose (dotted line) at 50 mV/s.

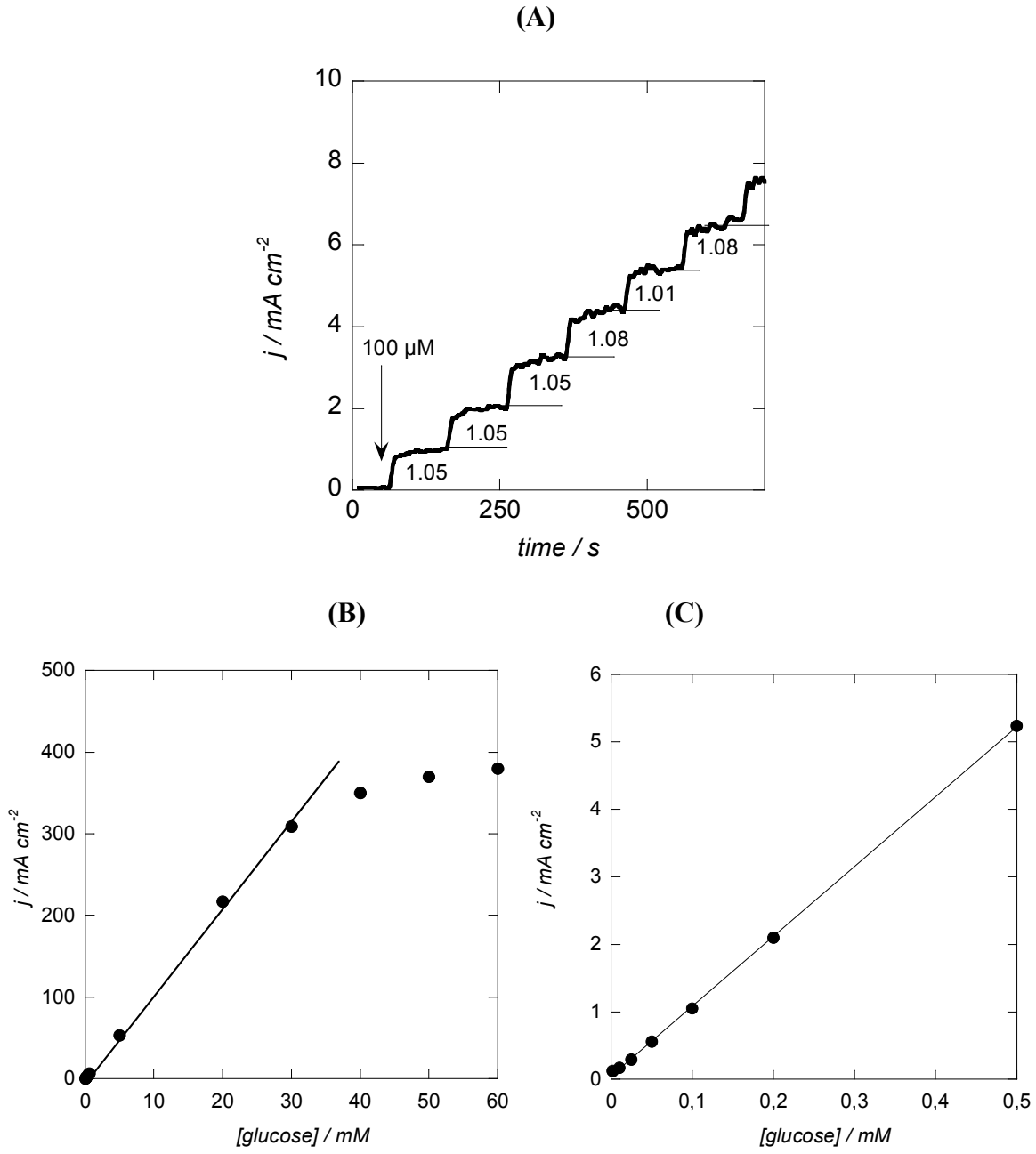

Figure 6: (A) Amperometric response curve of rGO/$Ni(OH)_2$ modified gold electrode polarized at +0.6 V vs. Ag/AgCl with successive additions of 100 µM glucose in 0.1 M NaOH; (B, C) Calibration curves for rGO/$Ni(OH)_2$ modified gold electrodes for the determination of glucose.

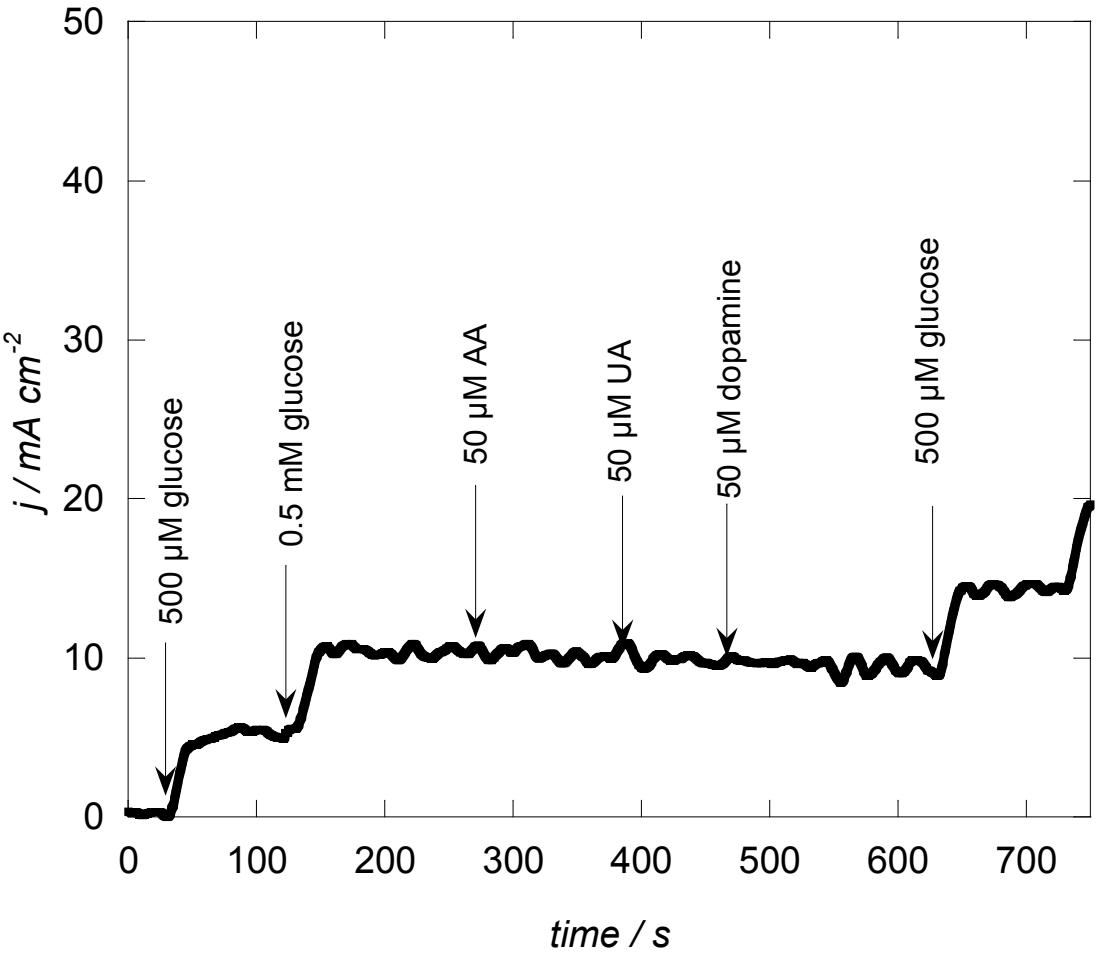

Figure 7: Interference test of rGO/Ni(OH)$_2$ modified gold electrodes in 0.1 M NaOH at +0.6 V with 0.5 mM glucose in the presence 0.05 mM ascorbic acid (AA), 0.05 mM uric acid (UA) and 0.05 mM dopamine.